Definition of displacement probability and diffusion time in *q*-space magnetic resonance measurements that use finite-duration diffusion-encoding gradients

Nicolas F. Lori,[a,b,*] Thomas E. Conturo,[a] and Denis Le Bihan[b]

[a] *Mallinckrodt Institute of Radiology, Washington University School of Medicine, 4525 Scott Ave., St. Louis, MO 63110, USA*
[b] *Service Hospitalier Frederic Joliot, CEA, 4 Place du General Leclerc, 91401 Orsay Cedex, France*

Abstract

In *q*-space diffusion NMR, the probability $P(\mathbf{r}, t_d)$ of a molecule having a displacement $\mathbf{r}$ in a diffusion time t_d is obtained under the assumption that the diffusion-encoding gradient $\mathbf{g}$ has an infinitesimal duration. However, this assumption may not always hold, particularly in human MRI where the diffusion-encoding gradient duration δ is typically of the same order of magnitude as the time offset Δ between encoding gradients. In this case, finite-δ effects complicate the interpretation of displacement probabilities measured in *q*-space MRI, and the form by which the signal intensity relates to them. By considering the displacement-specific dephasing, $\langle \mathbf{r} | e^{i\phi} \rangle$, of a set of spins accumulating a constant displacement vector $\mathbf{r}$ in the total time $\Delta + \delta$ during which diffusion is encoded, the probability recovered by a finite-δ *q*-space experiment can be interpreted. It is shown theoretically that a data analysis using a modified *q*-space index $\tilde{\mathbf{q}} = \gamma \delta \eta \mathbf{g}$, with γ the gyromagnetic ratio and $\eta = \sqrt{(\Delta - \delta/3)/(\Delta + \delta)}$, recovers the correct displacement probability distribution if diffusion is multi-Gaussian free diffusion. With this analysis, we show that the displacement distribution $P(\mathbf{r}, t_{exp})$ is measured at the experimental diffusion-encoding time $t_{exp} = \Delta + \delta$, and not at the reduced diffusion time $t_r = \Delta - \delta/3$ as is generally assumed in the NMR and MRI literature. It is also shown that, by defining a probability $\mathbf{P}(\mathbf{y}, \Delta)$ that a time $t < \delta$ exists such that a displacement $\mathbf{y}$ occurs from time t to $t + \Delta$, it is possible to describe the physical significance of the result obtained when we use the *q*-space formalism valid for infinitesimal δ when δ is not infinitesimal. These deductions were confirmed by simulations for homogeneous Gaussian diffusion and for heterogeneous diffusion in permeable microscopic Gaussian domains that are homogeneous on the μm scale. The results also hold for diffusion inside restricted spherical reflecting domains, but only if the radius of the domain is larger than a critical size. The simulations of the displacement-specific dephasing obtain that if $\delta > \delta_c$ then $\eta \neq \sqrt{(\Delta - \delta/3)/(\Delta + \delta)}$ which implies that we can no longer obtain the correct displacement probability from the displacement distribution. In the case that $|\mathbf{g}| = 18$ mT/m and $\Delta - \delta = 5$ ms, the parameter δ_c in ms is given by "$\delta_c = 0.49a^2 + 0.24$" where a is the sphere's radius expressed in μm. Simulation of *q*-space restricted diffusion MRI experiments indicate that if $\eta = \sqrt{(\Delta - \delta/3)/(\Delta + \delta)}$, the recovered displacement probability is always better than the Gaussian approximation, and the measured diffusion coefficient matches the diffusion coefficient at time $t_{exp} = \Delta + \delta$ better than it matches the diffusion coefficient at time $t_r = \Delta - \delta/3$. These results indicate that *q*-space MRI measurements of displacement probability distributions are theoretically possible in biological tissues using finite-duration diffusion-encoding gradients provided certain compartment size and diffusion encoding gradient duration constraints are met.
© 2003 Elsevier Inc. All rights reserved.

Keywords: Diffusion MRI; *q*-space; Diffusion time; Displacement probability; Finite-duration gradients; Restricted diffusion

1. Introduction

Diffusion MRI (DMRI) enables the study of water diffusion in a variety of environments (e.g. porous materials, gases and biological tissues). A pulse-sequence that is often used in DMRI is the pulsed-gradient spin

echo (PGSE) or Stejskal–Tanner sequence [1] in which diffusion-encoding gradients are applied before and after a 180° spin-echo refocusing pulse. The relevant diffusion-encoding parameters are the size and direction of the diffusion-encoding gradient vector, **g**, the time difference between the onset of the two diffusion-encoding gradients, Δ, and the duration of each of the diffusion-encoding gradients, δ. Several methods have been developed to analyze the MR signal intensity expected by this encoding. In the case of Gaussian diffusion, one can either solve the Torrey–Bloch equation [1], use the Gaussian phase dispersion [2–4], or use the center of mass approach [5].

In NMR of small samples, hardware with high gradient strengths can be used so that the time δ can be chosen to meet the condition $\delta \ll \Delta$. In this case it is straightforward to obtain the probability $P(\mathbf{r}, t_{\mathrm{d}})$ of a water molecule accumulating a net displacement **r** over the diffusion time t_{d}. This displacement probability is calculated by making an inverse Fourier transformation of the signal intensities measured with different **g** in a q-space imaging experiment [6–11], where the diffusion encoding time is given by Δ, and the q-space Fourier transform index is given by the vector $\mathbf{q} = \gamma\delta\mathbf{g}$ where γ is the gyromagnetic ratio.

In human MRI experiments, gradient strengths are limited and, to compensate, δ is typically lengthened to be on the order of Δ (e.g., $\delta = 25\,\mathrm{ms}$ and $\Delta = 31\,\mathrm{ms}$ in [11]). Under such conditions of finite-duration diffusion-encoding gradients (finite-δ), the probability distributions measured in q-space imaging are not necessarily valid, and the interpretation of the true diffusion time at which the probability distribution is measured is complicated [7, p. 364].

Several authors have provided methods that enable determination of the MR signal intensity from a known form of the displacement distribution (the "forward problem") in the finite-δ case. However, all these methods have drawbacks, and none enable solution of the "inverse problem" of measuring the probability distribution from the MR signal intensities. Some papers [12,13] consider that, instead of Δ, the diffusion time is actually the reduced diffusion time $t_{\mathrm{r}} = \Delta - \delta/3$. This assignment is based on taking the Fourier transform of the Stejskal–Tanner signal intensity equation, which replaces the experimental diffusion encoding time $\Delta + \delta$ with the reduced time $t_{\mathrm{r}} = \Delta - \delta/3$ inside the Gaussian probability expression. However, the terminology of this method is misleading, because the effect of the pulse sequence parameters of gradient encoding timings "$-(4/3)\delta$" is imparted to a biological parameter related to intrinsic diffusion displacement probability, rather than to an NMR pulse sequence parameter related to phase shifts [see [14] for discussion]. Furthermore, it is unclear why an increase in the duration δ would cause a reduction in the true diffusion time, as

predicted in this method. Therefore, it is not necessarily valid to equate the reduced diffusion time to the experimental diffusion-encoding time experienced by the water molecule. The *propagator method* [15–18] calculates the MR signal intensity by dividing the diffusion-encoding gradient time δ into infinitesimal time intervals. Then it chooses each pair of infinitesimal time intervals belonging to different diffusion-encoding gradients and considers that they behave like infinitesimal-δ q-space imaging experiments. Finally, it integrates over the contribution of all infinitesimal time intervals to obtain the MR signal intensity. This method has provided great help in understanding the structure of pores [15–18], but does not enable obtaining the displacement distribution from the MR signal intensities. In a third approach of *analytical calculation of total dephasing*, the total signal attenuation over the entire spin population is derived under certain conditions by assuming that there is a known probability expression for diffusive accumulation of a phase shift [2–4]. This approach enables a valid Fourier-like inverse transformation, but such a transformation provides a probability of evolving a phase shift rather than a probability of displacement.

In this paper we analyze the dephasing process and describe two basic physical ways of treating the diffusion phenomenon in probability terms for the finite-δ case. The first is the transport probability interpretation, which only depends on time Δ, and is very similar to the *analytical calculation of total dephasing* developed by Stepisnik [2–4]. The second defines the more traditional displacement probability, but does so under the assumption that it is possible to define the average of the displacement-specific dephasing.

By simple statistical analysis, we obtain the form of the average of the displacement-specific dephasing in the case of homogeneous non-restricted Gaussian diffusion [19]. We then made simulations to study the range of applicability of this formalism for the case of non-homogeneous non-restricted diffusion, and restricted diffusion inside a spherical domain. Finally, we simulated a q-space diffusion MR experiment for the case of homogeneous diffusion inside an impermeable sphere.

2. Theory

2.1. General analysis of the dephasing in a DMRI experiment

The average dephasing of a spin population in an MR experiment can be visualized in several different ways. The different visualizations of dephasing open different windows on the dynamics of the water molecules causing the dephasing phenomenon. Consider a water molecule moving between times $t = 0$ and $t = \mathrm{TE}$, with TE

the echo-time, and having a three-dimensional spatial location $\mathbf{r}(t)$ at time t.

There are several ways of defining displacement probabilities. First, there is the physical displacement probability, which is the actual displacement probability of the water molecules, and then there is the MR signal-defined displacement probability, which is inferred from the data by analyzing the intensity of the MR signal for different experimental parameters. The method for obtaining the MR signal-defined displacement probability is typically q-space MR [10,20,21], with $\mathbf{g}$ being the parameter that is varied.

We will consider two basic types of physical displacement probabilities. The first type is the probability density that there exist time moments t within the period of operation of the first diffusion-encoding gradient such that a water molecule undergoes a displacement $\mathbf{y}$ from time t to $t + \Delta$, given by $\mathbf{y} = \mathbf{r}(t + \Delta) - \mathbf{r}(t)$. This probability is indicated as $\mathbf{P}_\rho(\mathbf{y}, \Delta)$. In a PGSE experiment, this probability is identical to the probability of obtaining a phase shift $\phi = \mathbf{q} \cdot \mathbf{y}$ for infinitesimal time slices of the diffusion-encoding gradients at time t and $t + \Delta$ (see [2] for a description of phase shift probability), where $\mathbf{q} = \gamma\delta\mathbf{g}$. In the second definition of physical displacement probability, the probability density that a water molecule has displacement $\mathbf{r} = \mathbf{r}_\mathrm{f} - \mathbf{r}_\mathrm{o}$ during the entire time of the diffusion experiment is $P_\rho(\mathbf{r}, t_{\exp})$, where $\mathbf{r}_\mathrm{o}$ is the location of the water molecule at the onset of the first diffusion-encoding gradient, $\mathbf{r}_\mathrm{f}$ is the location after termination of the second diffusion-encoding gradient, and $t_{\exp}$ is the total encoding time of the diffusion experiment between the onset of the first gradient and the termination of the second gradient (i.e., $\Delta + \delta$). Diffusion MRI usually assumes to be measuring this second probability, but at diffusion time t_r instead of $t_{\exp}$. We will attempt to clarify the displacement probability that is measured in a finite-δ q-space MRI experiment using these two basic probability definitions.

In a PGSE experiment, the relevant parameter that is measured is the attenuation of signal in the MRI voxel or NMR sample induced by the diffusion-encoding gradients, given by the average dephasing $\langle \mathrm{e}^{\mathrm{i}\phi} \rangle$ of the spins of the water molecules in the sample or voxel:

$$\langle \mathrm{e}^{\mathrm{i}\phi} \rangle = \frac{I_{\mathbf{g},\Delta,\delta}}{I_0}. \tag{1}$$

In Eq. (1), $I_{\mathbf{g},\Delta,\delta}$ is the MR signal intensity that is a function of $\mathbf{g}$, Δ, and δ, obtained with diffusion-encoding gradient $\mathbf{g}$ of duration δ with an offset Δ between the two diffusion-encoding gradients; and I_0 is the MR signal intensity obtained in the absence of diffusion-encoding gradients. Eq. (1) assumes that all effects from background gradients are multiplicative and identical for I_0 and $I_{\mathbf{g},\Delta,\delta}$.

If the experimental medium is not homogeneous, the displacement probability densities will depend on the location of the starting point $\mathbf{r}_\mathrm{o}$. It might also occur that the water density $\rho(\mathbf{r}_\mathrm{o})$ will not be constant throughout the medium. For each of the two definitions of displacement probability, there is a corresponding relation between the average dephasing and the probability density according to

$$\langle \mathrm{e}^{\mathrm{i}\phi} \rangle = \int_{-\infty}^{\infty} \rho(\mathbf{y}_\mathrm{o}) \int_{-\infty}^{\infty} \mathbf{P}_\rho(\mathbf{y}_\mathrm{f}, \mathbf{y}_\mathrm{o}, \Delta) \mathrm{e}^{\mathrm{i}\mathbf{q}\cdot(\mathbf{y}_\mathrm{f}-\mathbf{y}_\mathrm{o})} \mathrm{d}\mathbf{y}_\mathrm{f}\mathrm{d}\mathbf{y}_\mathrm{o} \tag{2}$$

and

$$\langle \mathrm{e}^{\mathrm{i}\phi} \rangle = \int_{-\infty}^{\infty} \rho(\mathbf{r}_\mathrm{o}) \int_{-\infty}^{\infty} P_\rho(\mathbf{r}_\mathrm{f}, \mathbf{r}_\mathrm{o}, t_{\exp}) \langle \mathbf{r}_\mathrm{f}, \mathbf{r}_\mathrm{o} | \mathrm{e}^{\mathrm{i}\phi} \rangle \mathrm{d}\mathbf{r}_\mathrm{f}\mathrm{d}\mathbf{r}_\mathrm{o}, \tag{3}$$

where $\langle \mathbf{r}_\mathrm{f}, \mathbf{r}_0 | \mathrm{e}^{\mathrm{i}\phi} \rangle$ is the average signal attenuation for a group of spins starting at location $\mathbf{r}_0$ and ending at location $\mathbf{r}_\mathrm{f}$, and where the integrals are over infinite three-dimensional space. In Eq. (2), $\mathbf{P}_\rho(\mathbf{y}_\mathrm{f}, \mathbf{y}_\mathrm{o}, \Delta)$ relates to the probability of acquiring a specific phase shift $\mathrm{e}^{\mathrm{i}\mathbf{q}(\mathbf{y}_\mathrm{f}-\mathbf{y}_\mathrm{o})}$ (analogous to the phase shift probability in [2]), and describes the behavior of time slices of the diffusion encoding experiment offset by Δ, similar to the analysis in the propagator method [15]. In Eq. (3), use of the displacement-specific dephasing factor $\langle \mathbf{r}_\mathrm{f}, \mathbf{r}_\mathrm{o} | \mathrm{e}^{\mathrm{i}\phi} \rangle$ provides a necessary link between the displacement probability and the dephasing that enables the integral to be written.

If the displacement-specific dephasing $\langle \mathbf{r}_\mathrm{f}, \mathbf{r}_0 | \mathrm{e}^{\mathrm{i}\phi} \rangle$ only depends on the net displacement $\mathbf{r} = \mathbf{r}_\mathrm{f} - \mathbf{r}_0$ (this will later be shown to be the case in Gaussian free diffusion and in certain cases of restricted diffusion), then we define the average of the displacement-specific dephasing as $\langle \mathbf{r} | \mathrm{e}^{\mathrm{i}\phi} \rangle$. Then, using Eqs. (2) and (3), we define

$$\mathbf{P}(\mathbf{y}, \Delta) = \int_{-\infty}^{\infty} \rho(\mathbf{y}_\mathrm{o}) \mathbf{P}_\rho(\mathbf{y} + \mathbf{y}_\mathrm{o}, \mathbf{y}_\mathrm{o}, \Delta) \mathrm{d}\mathbf{y}_\mathrm{o} \tag{4}$$

and

$$P(\mathbf{r}, t_{\exp}) = \int_{-\infty}^{\infty} \rho(\mathbf{r}_\mathrm{o}) P_\rho(\mathbf{r} + \mathbf{r}_\mathrm{o}, \mathbf{r}_\mathrm{o}, t_{\exp}) \mathrm{d}\mathbf{r}_\mathrm{o}. \tag{5}$$

Applying Eqs. (4) and (5) to Eqs. (2) and (3), respectively, we obtain

$$\langle \mathrm{e}^{\mathrm{i}\phi} \rangle = \int_{-\infty}^{\infty} \mathbf{P}(\mathbf{y}, \Delta) \mathrm{e}^{\mathrm{i}\mathbf{q}\cdot\mathbf{y}} \mathrm{d}\mathbf{y} \tag{6}$$

and

$$\langle \mathrm{e}^{\mathrm{i}\phi} \rangle = \int_{-\infty}^{\infty} P(\mathbf{r}, t_{\exp}) \langle \mathbf{r} | \mathrm{e}^{\mathrm{i}\phi} \rangle \mathrm{d}\mathbf{r}. \tag{7}$$

Comparing Eqs. (6) and (7), and noting that the integration variables are dummy variables with identical integration ranges that are symmetric about the origin in three-dimensional space, we obtain a relation between the even-symmetric part of the two definitions of displacement probabilities:

$$\text{Sym}[\mathbf{P}(\mathbf{r}, \Delta)\mathrm{e}^{\mathrm{i}\mathbf{q}\cdot\mathbf{r}}] = \text{Sym}[P(\mathbf{r}, t_{\exp})\langle\mathbf{r}|\mathrm{e}^{\mathrm{i}\phi}\rangle]. \tag{8}$$

This expression provides some understanding of the relation between $\mathbf{P}(\mathbf{y}, \Delta)$ and $P(\mathbf{r}, t_{\exp})$, where "Sym" is the symmetric part of a function.

If the displacement probabilities $\mathbf{P}(\mathbf{y}, \Delta)$ and $P(\mathbf{r}, t_{\exp})$ are zero-centered even symmetric, as expected in diffusion, Eqs. (6) and (7) become

$$\langle\mathrm{e}^{\mathrm{i}\phi}\rangle = \int_{-\infty}^{\infty} \mathbf{P}(\mathbf{y}, \Delta)\cos(\mathbf{q}\cdot\mathbf{y})\mathrm{d}\mathbf{y} \tag{9}$$

and

$$\langle\mathrm{e}^{\mathrm{i}\phi}\rangle = \int_{-\infty}^{\infty} P(\mathbf{r}, t_{\exp})\text{Sym}\langle\mathbf{r}|\mathrm{e}^{\mathrm{i}\phi}\rangle\mathrm{d}\mathbf{r}. \tag{10}$$

When MRI q-space imaging is performed using finite-δ diffusion-encoding gradients, and the data are analyzed using standard q-space methods, the MR signal-defined displacement probability $P_{\mathrm{MR}}(\mathbf{r}, t_{\mathrm{r}})$ as defined in [10,20,21] is:

$$P_{\mathrm{MR}}(\mathbf{r}, t_{\mathrm{r}})_{\mathbf{q}} = \int_{-\infty}^{\infty} \langle\mathrm{e}^{\mathrm{i}\phi}\rangle_{\Delta,\delta,\mathbf{g}}\cos(\mathbf{q}\cdot\mathbf{r})\mathrm{d}\mathbf{q}. \tag{11}$$

For the case of general (non-Gaussian) displacement distributions, Eqs. (9) and (10) can be compared to Eq. (11) to obtain, respectively,

$$P_{\mathrm{MR}}(\mathbf{r}, t_{\mathrm{r}})_{\mathbf{q}} = \mathbf{P}(\mathbf{r}, \Delta) \tag{12}$$

and, using $\mathbf{u}$ as a displacement integration variable,

$$P_{\mathrm{MR}}(\mathbf{r}, t_{\mathrm{r}})_{\mathbf{q}} = \int_{-\infty}^{\infty}\int_{-\infty}^{\infty} P(\mathbf{u}, t_{\exp})\text{Sym}\langle\mathbf{u}|\mathrm{e}^{\mathrm{i}\phi}\rangle$$
$$\times \cos(\mathbf{q}\cdot\mathbf{r})\mathrm{d}\mathbf{u}\,\mathrm{d}\mathbf{q}. \tag{13}$$

The problem in Eqs. (11)–(13) is that three different diffusion times (t_{r}, Δ, and $t_{\exp}$) appear in those equations, which makes it very difficult to assign a single diffusion time to the experiment. Of these three diffusion times, the most problematic is t_{r} for its physical meaning is unclear.

To relate $P_{\mathrm{MR}}(\mathbf{r}, t_{\mathrm{r}})$ with $P(\mathbf{r}, t_{\exp})$ it is necessary and sufficient to know $\text{Sym}\langle\mathbf{r}|\mathrm{e}^{\mathrm{i}\phi}\rangle$. In the next section, we derive $\text{Sym}\langle\mathbf{r}|\mathrm{e}^{\mathrm{i}\phi}\rangle$ for the case of Gaussian diffusion.

2.2. Finite δ q-space imaging for unrestricted Brownian motion (Gaussian diffusion)

The average signal attenuation in a voxel for a Stejskal–Tanner experiment with the diffusion experiment encoding time $t_{\exp}$ is given by [1,3,4]

$$\langle\mathrm{e}^{\mathrm{i}\phi}\rangle_{\Delta,\delta,\mathbf{g}} = \mathrm{e}^{-(\gamma\delta\mathbf{g})^{\mathrm{T}}\hat{\mathbf{D}}(\gamma\delta\mathbf{g})[\Delta-\delta/3]}, \tag{14}$$

where $\hat{\mathbf{D}}$ is the diffusion tensor, which is a function of the time-dependent random acceleration vector $\mathbf{A}$ (with $\otimes$ the symbol for vector product) and the friction tensor $\hat{\zeta}$, defined in [22] as

$$\hat{\mathbf{D}} = \left[\hat{\zeta}^{-1}\right]^{\mathrm{T}} \frac{\int_{-\infty}^{\infty} \mathrm{d}\tau\langle\mathbf{A}^{\mathrm{T}}(\tau)\otimes\mathbf{A}(0)\rangle}{6}\left[\hat{\zeta}^{-1}\right]. \tag{15}$$

We propose a modified q-space index $\tilde{\mathbf{q}} \equiv \eta\mathbf{q}$ whereupon, if $P(\mathbf{r}, t_{\exp})$ is a zero-centered Gaussian distribution with variance equal to $[2\hat{\mathbf{D}}t_{\exp}]^{-1}$, the Fourier transform [23] of $P(\mathbf{r}, t_{\exp})$ is:

$$\mathscr{F}[P(\mathbf{r}, t_{\exp})]_{\mathbf{r}}\big(\tilde{\mathbf{q}}\big) = \int_{-\infty}^{\infty} (2\pi)^{-3/2}\big|2\hat{\mathbf{D}}t_{\exp}\big|^{-1/2}$$
$$\times \mathrm{e}^{-\frac{1}{2}\mathbf{r}\cdot[2\hat{\mathbf{D}}t_{\exp}]^{-1}\cdot\mathbf{r}}\cos(\eta\mathbf{q}\cdot\mathbf{r})\mathrm{d}\mathbf{r}$$
$$= \mathrm{e}^{-(\gamma\delta\mathbf{g})^{\mathrm{T}}\hat{\mathbf{D}}(\gamma\delta\mathbf{g})(\eta^2 t_{\exp})}. \tag{16}$$

Because Eq. (16) must agree with Eq. (14) in the case of Gaussian diffusion, we obtain that η defined as

$$\eta = \frac{\cos^{-1}[\text{Sym}\langle\mathbf{r}|\mathrm{e}^{\mathrm{i}\phi}\rangle]}{\mathbf{q}\cdot\mathbf{r}}$$

where $\cos^{-1}$ is the inverse of the cosine function, is given by:

$$\eta = \sqrt{\frac{\Delta - \delta/3}{t_{\exp}}}. \tag{17}$$

Combining Eqs. (10), (14), (16) and (17) we obtain

$$\langle\mathrm{e}^{\mathrm{i}\phi}\rangle = \int_{-\infty}^{\infty} P(\mathbf{r}, t_{\exp})\cos\left(\gamma\delta\sqrt{\frac{\Delta-\delta/3}{t_{\exp}}}\mathbf{g}\cdot\mathbf{r}\right)\mathrm{d}\mathbf{r}. \tag{18}$$

The inverse Fourier transform [23] of Eq. (18) can then be taken to provide a means for measuring $P_{\mathrm{MR}}(\mathbf{r}, t_{\exp})_{\tilde{\mathbf{q}}}$ in q-space imaging according to

$$P_{\mathrm{MR}}(\mathbf{r}, t_{\exp})_{\tilde{\mathbf{q}}} = \mathscr{F}^{-1}\left[\langle\mathrm{e}^{\mathrm{i}\phi}\rangle_{\Delta,\delta,\mathbf{g}}\right]_{\tilde{\mathbf{q}}}(\mathbf{r})$$
$$= (2\pi)^{-3/2}\int_{-\infty}^{\infty} \langle\mathrm{e}^{\mathrm{i}\phi}\rangle_{\Delta,\delta,\mathbf{g}}\cos\left(\tilde{\mathbf{q}}\cdot\mathbf{r}\right)\mathrm{d}\tilde{\mathbf{q}}. \tag{19}$$

It is later shown that Eq. (19) is valid even if we have heterogeneous Gaussian diffusion with macroscopic or microscopic Gaussian domains, and even in the case of spherically restricted diffusion provided the compartment size is not too small.

Comparing Eq. (18) with Eq. (7) and assuming that $P(\mathbf{r}, t_{\exp})$ is symmetric, we obtain:

$$\text{Sym}\langle\mathbf{r}|\mathrm{e}^{\mathrm{i}\phi}\rangle = \cos\left(\sqrt{\frac{\Delta-\delta/3}{t_{\exp}}}\gamma\delta\mathbf{g}\cdot\mathbf{r}\right). \tag{20}$$

Because $\langle\mathbf{r}|\mathrm{e}^{\mathrm{i}\phi}\rangle$ is complex-valued and because of Eq. (8), then when Eq. (20) holds we must have $\text{Sym}\langle\mathbf{r}|\mathrm{e}^{\mathrm{i}\phi}\rangle = \text{Re}\langle\mathbf{r}|\mathrm{e}^{\mathrm{i}\phi}\rangle$ and $\text{Asym}\langle\mathbf{r}|\mathrm{e}^{\mathrm{i}\phi}\rangle = \text{Im}\langle\mathbf{r}|\mathrm{e}^{\mathrm{i}\phi}\rangle$ where "Asym" is the anti-symmetric part of the function. This implies that $\text{Asym}\langle\mathbf{r}|\mathrm{e}^{\mathrm{i}\phi}\rangle = \sin(\iota\gamma\delta\mathbf{g}\cdot\mathbf{r})$ where ι is not necessarily equal to η.

As said in the Introduction, it is expected that $t_{\exp} = \Delta + \delta$. To confirm this, we did a simulation of Brownian motion [22]. In that Brownian motion simulation, we used the result that, for non-infinitesimal time-scales (i.e., time-scales corresponding to displacements bigger than the nanometer), a Brownian motion

with the above-mentioned characteristics behaves as a random walk with diffusion tensor $\hat{\mathbf{D}}$ defined by Eq. (15). In that three-dimensional random walk, the three dimensions are considered separately. For each direction (the z-direction for example), and for each time-step δ/L, the molecule will have a displacement with magnitude $\sqrt{2\hat{\mathbf{z}}^{\mathbf{T}} \cdot \hat{\mathbf{D}} \cdot \hat{\mathbf{z}}\delta/L}$. The probability of having positive displacements or negative displacements is the same, and is independent for each of the three dimensions (notice that in the case of restricted diffusion, the equivalence of positive and negative displacement probability is not valid near the boundary).

We then analyzed the shape of the real and imaginary parts of $\langle \mathbf{r}|e^{i\phi}\rangle$ and confirmed that $\mathrm{Sym}\langle \mathbf{r}|e^{i\phi}\rangle = \mathrm{Re}\langle \mathbf{r}|e^{i\phi}\rangle$ and $\mathrm{Asym}\langle \mathbf{r}|e^{i\phi}\rangle = \mathrm{Im}\langle \mathbf{r}|e^{i\phi}\rangle$. Using $\mathrm{Re}\langle \mathbf{r}|e^{i\phi}\rangle$, we were able to confirm Eq. (20) with $t_{\exp} = \Delta + \delta$ within statistical error (see Results), which obtains the final form of Eqs. (17) and (20) for mono-Gaussian free diffusion:

$$\eta = \sqrt{\frac{\Delta - \delta/3}{\Delta + \delta}} \qquad (21)$$

and

$$\mathrm{Sym}\langle \mathbf{r}|e^{i\phi}\rangle = \mathrm{Re}\langle \mathbf{r}|e^{i\phi}\rangle$$
$$= \cos\left(\gamma\delta\sqrt{\frac{\Delta - \delta/3}{\Delta + \delta}}\mathbf{g} \cdot \mathbf{r}\right). \qquad (22)$$

Because Eqs. (21) and (22) do not depend on the diffusion tensor, there is no reason that those equations would depend on $\mathbf{r}_0$ even if the diffusion process is not mono-Gaussian. Simulations in later sections further strengthen this point in the case of heterogeneous, non-restricted Gaussian diffusion. In the case of restricted diffusion, we obtain that Eq. (22) still holds provided the restricted domain is large enough.

Combining Eqs. (10) and (22), in the cases that Eq. (22) is valid, we obtain that:

$$P(\mathbf{r}, \Delta + \delta) = \int_{-\infty}^{\infty} \langle e^{i\phi}\rangle_{\Delta,\delta,\mathbf{g}} \cos\left(\gamma\delta\sqrt{\frac{\Delta - \delta/3}{\Delta + \delta}}\mathbf{g} \cdot \mathbf{r}\right)$$
$$\times \mathrm{d}\left[\gamma\delta\sqrt{\frac{\Delta - \delta/3}{\Delta + \delta}}\mathbf{g}\right]. \qquad (23)$$

Because the right-hand sides of Eqs. (23) and (19) are identical, we have therefore shown that, in the case where Eq. (22) is valid, the MR-observed probability is given by

$$P_{\mathrm{MR}}\left(\mathbf{r}, t_{\exp}\right)_{\tilde{\mathbf{q}}} = P(\mathbf{r}, \Delta + \delta). \qquad (24)$$

The Fourier transformation in Eq. (23) can be used to define a revised q-space formalism that gives valid results even when δ is finite, provided that Eq. (22) is valid. To apply this formalism, the investigator can vary δ, Δ, or $\mathbf{g}$ to cause variations in $\tilde{\mathbf{q}}$, and must index the intensities with the proper $\tilde{\mathbf{q}}$ prior to Fourier transformation

as in Eq. (23). Later in the Results section, using simulations of water diffusion, we demonstrate that Eq. (22) is valid in a large range of physical situations. As it is not possible to do an infinite number of signal attenuation measurements, in practice Eq. (23) would be approximated by a three-dimensional discrete sum (as it is done in standard q-space imaging, e.g. [11]).

The different values of $\tilde{\mathbf{q}}$ can be obtained in different ways, but the only way to vary $\tilde{\mathbf{q}}$ in a manner that is consistent with Eq. (23) and that yields a meaningful probability measurement is to fix $t_{\exp} = \Delta + \delta$. The simplest way to do this is to fix both Δ and δ, so that $\mathbf{g}$ is the only parameter that varies. In this case, Eq. (23) reduces to

$$P(\mathbf{r}, \Delta + \delta) = \sqrt{\frac{\Delta - \delta/3}{\Delta + \delta}} \int_{-\infty}^{\infty} \langle e^{i\phi}\rangle_{\Delta,\delta,\mathbf{g}}$$
$$\times \cos\left(\sqrt{\frac{\Delta - \delta/3}{\Delta + \delta}}\mathbf{q} \cdot \mathbf{r}\right)\mathrm{d}\mathbf{q} \qquad (25)$$

This expression has the typical appearance of conventional q-space analysis, with the exception of factors $\sqrt{(\Delta - \delta/3)/(\Delta + \delta)}$ that account for finite-δ effects. Eq. (25) reduces to the infinitesimal-δ q-space expression when $\delta \ll \Delta$.

3. Methods

3.1. Displacement-specific dephasing for homogenous Gaussian diffusion

We calculated $\mathrm{Re}\langle \mathbf{r}|e^{i\phi}\rangle$ and $\mathrm{Im}\langle \mathbf{r}|e^{i\phi}\rangle$ by numerically simulating the phase shifts accumulated by 3D random walks with homogeneous Gaussian diffusion occurring during a PGSE experiment having diffusion-encoding gradients along z. If the diffusion is homogeneously Gaussian, we know that $\mathrm{Re}\langle e^{i\phi}\rangle = e^{-\mathbf{q}\cdot\mathbf{D}\cdot\mathbf{q}[\Delta - \delta/3]}$ and $\mathrm{Im}\langle e^{i\phi}\rangle = 0$ [1]. This expected result was used to check on our simulations at various δ/Δ ratios. Subsets of random walks were chosen having fixed Z displacements, and these subsets were used to estimate the displacement-specific dephasings $\mathrm{Re}\langle \mathbf{r}|e^{i\phi}\rangle$ and $\mathrm{Im}\langle \mathbf{r}|e^{i\phi}\rangle$ as a function of the three-dimensional displacement $\mathbf{r}$ (it was only necessary to consider the z component of $\mathbf{r}$ because the gradient was along z). The observed $\mathbf{r}$ dependence of the simulated $\mathrm{Re}\langle \mathbf{r}|e^{i\phi}\rangle$ was then compared to the right-hand-side of Eq. (20) to confirm that Eqs. (21) and (22) are valid. The same analysis was done for the imaginary component to obtain the value for ι, although the functional form of the imaginary component cannot be determined by the theory herein (except for knowing that it must behave as a sine).

Unless otherwise stated, 800 random walks were simulated to calculate the displacement-specific dephasing at a given δ/Δ ratio. The simulations were repeated for different δ/Δ ratios. Each random walk was composed of

805 steps, having at each step a probability of stepping in direction $\mathbf{r}$ such that the diffusion tensor has eigenvalues $\lambda_z = 1.43 \times 10^{-3}$ mm^2/s, $\lambda_y = 0.49 \times 10^{-3}$ mm^2/s, and $\lambda_x = 0.25 \times 10^{-3}$ mm^2/s corresponding to the splenium of the corpus callosum as in [24]. The 800 random-walk trajectories were partitioned into 100 displacement bins (Z-bins). Each trajectory was assigned to one of the 100 Z-bins based on having a displacement between Z_0 and $Z_0 + \Delta Z$ along the diffusion-encoding gradient, with bin width $\Delta Z = 1$ μm. The bin locations Z_0 were half-integer multiples of ΔZ starting from $Z_0 = 0$, and spanning positive and negative directions. The phase shift caused by each step in the random walk was calculated as $\phi(\tau) = \gamma \mathbf{g}(\tau) \cdot \mathbf{r}(\tau) t_{\text{step}}$, where τ is the time at which the step occurs ($0 \leqslant \tau \leqslant$ TE), and t_{step} is the duration of each step. The total accumulated phase for a random walk was then $\phi(\text{TE}) = \sum_{\text{steps}} \phi(\tau)$. We then calculated the total counts (random walks) per bin, the mean position $\langle Z \rangle$ in the bin (not necessarily equal to Z_0), the attenuated real $\text{Re}\langle\langle Z \rangle | e^{i\phi}\rangle$ and imaginary $\text{Im}\langle\langle Z \rangle | e^{i\phi}\rangle$ signals in the bin, and the standard deviation (s.d.) of the component signal in the bin.

The calculated values $\text{Re}\langle\langle Z \rangle | e^{i\phi}\rangle$ and $\text{Im}\langle\langle Z \rangle | e^{i\phi}\rangle$ enabled the determination of η and ι using

$$\eta = \left\langle \frac{\cos^{-1}(\text{Re}\langle\langle Z \rangle | e^{i\phi}\rangle)}{\gamma g_z \langle Z \rangle} \right\rangle$$

and

$$\iota = \left\langle \frac{\sin^{-1}(\text{Im}\langle\langle Z \rangle | e^{i\phi}\rangle)}{\gamma g_z \langle Z \rangle} \right\rangle,$$

respectively, where the average that calculates η and ι is an average over different values of $\langle Z \rangle$. The η and ι were calculated for each different setting of $\varepsilon = \delta/\Delta$. Also at each ε, an experimental parameter χ was determined such that $\eta = \sqrt{(\Delta - \delta/3)(\Delta + \chi\delta)}$ in order to calculate an observed diffusion encoding time $t_{\text{obs}} = \Delta + \chi\delta$.

3.2. Displacement-specific dephasing in fully permeable Gaussian diffusion domains

The diffusion properties of a biological tissue are not usually homogeneous. Therefore, it makes sense to include the existence of domains in simulations of diffusion processes. The domains that we will consider are cubic with half sides ranging from 1 μm to 1 mm, and the diffusion properties within a domain are homogeneous and Gaussian. The diffusion properties of each domain were obtained by multiplying each of the three diagonal elements of the diffusion tensor used in the homogeneous case by a uniformly distributed random number ranging from 0.5 to 2.0. The starting point of the random walk was always located at the center of the same home domain, and the trajectories were allowed to pass freely between the home domain and neighboring domains. The assignment of diffusion properties in each

domain was constant for the different trajectories. Because the water molecules move for 10 ms before the onset of the diffusion-encoding gradient, the initiation at the center of the domain is not expected to bias the simulation results. Because some of the steps in the calculation of η required the division by the total displacement of a trajectory, no trajectory should have a total net displacement that is absolutely equal to 0. The method we found to guarantee non-zero net displacements was to multiply each Markov step by a Gaussian random variable with mean 1 and standard deviation 0.01. This way of defining the Markov steps was also used in the restricted diffusion simulations that are described in the next section.

3.3. Displacement-specific dephasing in impermeable spherical restricted domains

In biological tissues and porous media, there are often restricted domains that cannot be represented by the permeable domains of the previous section. Therefore, the validity of Eq. (22) needs to be tested in the restricted case. In the simulations of a spherical restricted domain, the center of the domain was located at [$x = 0$, $y = 0$, $z = 0$] and the radius of the sphere was a, with a ranging from 1 μm to 1 mm. Because the location of the starting point might in this case be very relevant, the starting point was a random variable that was uniformly distributed within the sphere, and the time between the start of the trajectory and the start of the diffusion-encoding gradient was reduced to 2 ms. Identically to what occurred in the simulations of permeable domains, the starting domain properties are the same for all trajectories. Because in this case the water molecules were confined to the same domain, the diffusion properties were the same for all trajectories and in all simulation cases. In the restricted domain simulations, the number of trajectories was 2000 and the number of steps during t_{exp} was 2000 (unless otherwise stated). The values of η and ι were calculated as in the other simulation cases, and the diffusion coefficient D was calculated by

$$D = -\frac{1}{(\gamma|\mathbf{g}|\delta)^2(\Delta - \delta/3)} \log\left[\langle e^{i\phi}\rangle\right] \tag{26}$$

at each setting of δ and Δ. These simulations required 70 h of computer time using Matlab 5.2 (Mathworks, Natick, MA, USA) running on a Sun V880 computer (Sun Microsystems Inc., Santa Clara, CA, USA) with 900 MHz processors and 16 GB RAM. If Gaussian diffusion is a valid approximation, one could calculate the diffusion coefficient as being equal to the average square displacement divided by twice the diffusion time. A comparison between the diffusion coefficient calculated using Eq. (26) and the diffusion coefficient calculated from the displacements for the diffusion times t_r and t_{exp} will be made.

3.4. Simulated restricted diffusion q-space imaging experiment

The previous section was concerned with the determination of the diffusion coefficient in a simulated restricted diffusion experiment. This section goes one step further, it does the same simulation as described in the previous section (with fewer trajectories) for 32 different co-linear values of **g**, with **g** in the direction of z varying from -144.0 to $144.0\,\mathrm{mT/m}$. The 32 simulated MR signal intensities are then Fourier transformed using our altered q-space formalism to define simulated recovered displacement distributions.

The q-space simulations have as their result, the rms error between the recovered displacement probability and the true displacement probability, with the mean being taken across different values of z. These simulations required 221 h of computer time using Matlab 5.2 (Mathworks, Natick, MA, USA) running on a Sun V880 computer (Sun Microsystems Inc., Santa Clara, CA, USA) with 900 MHz processors and 16 GB RAM.

4. Results

4.1. Displacement-specific dephasing in homogenous Gaussian diffusion

In Fig. 1A the displacement-specific real signal attenuation $\mathrm{Re}\langle\langle Z\rangle|\mathrm{e}^{\mathrm{i}\phi}\rangle$ is graphed as a function of $\langle Z\rangle$ (red circles). The signal attenuation is normalized so that the maximum absolute value of both the real and imaginary components of the MR signal are equal to 1.0. Using only bins with counts greater than 5, we then fit a $\cos(\gamma\delta\eta g_z Z)$ function to the simulated real signals at each bin $\langle Z\rangle$ (dark blue curve fit to red circles in Fig. 1A), and a $\sin(\gamma\delta\iota g_z Z)$ function to the observed imaginary signal (magenta curve fit to green circles in Fig. 1B). Although it is expected that η is given by Eq. (21), the form of ι is not a priori known. The dashed cyan line in Fig. 1A is the curve that would occur if $\eta = 1$ (as in the infinitesimal-δ approximation). It is clear in Fig. 1A that the blue curve is very different from the dashed cyan line. This indicates that we should expect a simulation result different from $\eta = 1$. This simulation procedure was repeated for different values of δ/Δ, holding constant the time from the beginning of the first diffusion-encoding gradient to the end of the second diffusion-encoding gradient ($\Delta + \delta$). The η and ι obtained at each $\varepsilon = \delta/\Delta$ is graphed in Fig. 2, which indicates the validity of Eq. (21) and confirms the model in Eq. (22). The parameter χ was calculated at each ε such that $t_{\exp} = \Delta + \chi\delta$. By averaging all the χ values obtained at different ε, we obtained

$$t_{\mathrm{obs}} = \Delta + (1.05 \pm 0.10)\,\delta, \tag{27}$$

where the number in parentheses is the mean and standard error of the mean (SEM) for 39 different settings of ε. This result is in agreement with $t_{\exp} = \Delta + \delta$, which is the total time from the beginning to the end of the diffusion-encoding period.

4.2. Displacement-specific dephasing in permeable Gaussian diffusion domains

The behavior of η as a function of ε is expected to be in agreement with Eq. (21), in the case of diffusion
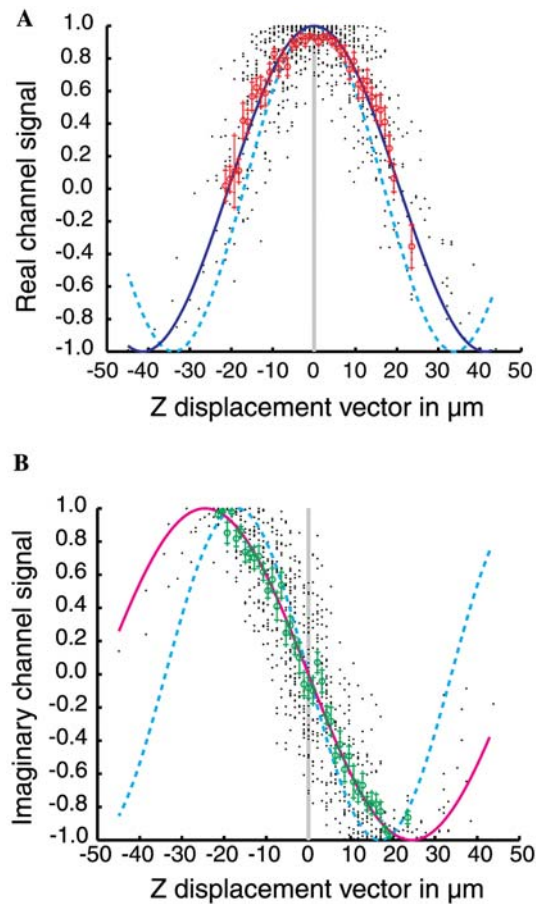
Fig. 1. Real (A) and imaginary (B) signals simulated for groups of spins having specific Z displacements. The circles and error bars (red in (A) and green in (B)) mark the simulated mean signals ± 1 SEM for a group of random walks having Z displacements that fall within a range of Z (a Z-bin). The signal values of individual random walks are shown as small black points, normalized to a maximum of 1.0. The real signal attenuations of the Z-bins were least-squares fit to a cosine function (blue curve in A), while the imaginary signal attenuations of the Z-bins were fit to a sine function (magenta curve in B). The dephasing curves that would be obtained for $\eta = 1$ and $\iota = 1$ are shown as dashed cyan curves in (A) and (B), respectively. The vertical gray lines mark the $Z = 0$ line of symmetry. The simulation assumed a PGSE pulse sequence with $\Delta = 44.80\,\mathrm{ms}$, $\delta = 15.75\,\mathrm{ms}$, and used random walks of 8050 steps. Note that this simulation was not used to calculate χ but simply illustrates the curve fitting process for data calculated using a large number of steps.
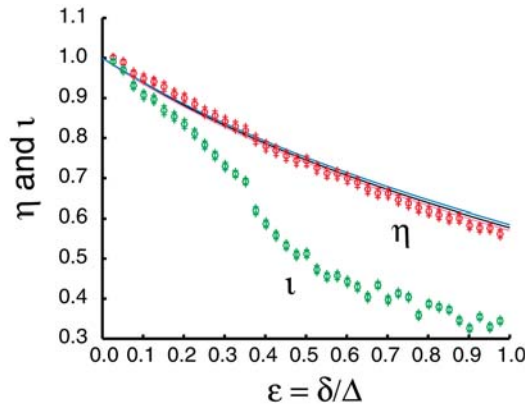
Fig. 2. Computation of the bin-averaged η and ι as a function of $\varepsilon = \delta/\Delta$, where $\Delta + \delta$ is held constant. The $\langle\eta\rangle$ (red circles) and $\langle\iota\rangle$ (green circles) were computed as described in the Methods section. The ideal curve for η at $\chi = 1$, $\eta = \sqrt{(\Delta - \delta/3)/(\Delta + \delta)}$, is given for reference (solid black line). The curves for η at the calculated value of $\chi = 1.05$ (magenta) and $\chi = 0.95$ (blue) are given also.

through permeable Gaussian domains. We observed that this was true for all domain sizes (cube half-sides a ranging from 1 to 1000 μm). In the extreme cases of $a = 1$ μm (Fig. 3A) and $a = 1$ mm (Fig. 3B), the match with Eq. (21) (blue line) is very good, confirming Eq. (22). This agreement was also very good for all intermediate cases (not shown).

4.3. Displacement-specific dephasing in an impermeable spherical restricted domain

For the case of non-restricted Gaussian diffusion, the behavior of η as a function of ε is in agreement with Eqs. (21), (22). But it is possible that for small restricted domains, and long diffusion-encoding times, the Eqs. (21), (22) are no longer valid. To test this possibility, we checked the validity of Eq. (21) for a range of domain sizes and diffusion-encoding times.

For a ranging from 1 to 10 μm, graphs depicting the behavior of η as a function of δ were generated. For $a = 4$ μm, $\eta(\delta)$ is graphed in Fig. 4A, with δ ranging from 0 to 30 ms, and "$\Delta - \delta = 5$ ms". For each value of a, the critical threshold δ_c was determined (see Fig. 4A), and a graph of $\delta_c(a)$ (Fig. 4B) was created. For all values of δ, $|\mathbf{g}| = 18$ mT/m. In Fig. 4B, we observe that $\delta_c = 0.49a^2 + 0.24$ with δ_c in ms and a in μm.

For a equal to 5, 10, and 15 μm, we then obtained the behavior of the diffusion coefficient defined as in Eq. (26) (blue stars in Fig. 5A for the case of $a = 10$ μm) as a function of δ. Also in Fig. 5A, we can observe the diffusion coefficient obtained using the same average square displacement approach and using the average square displacement at time t_r (dotted red line), and the diffusion coefficient obtained using the same average square displacement approach at time
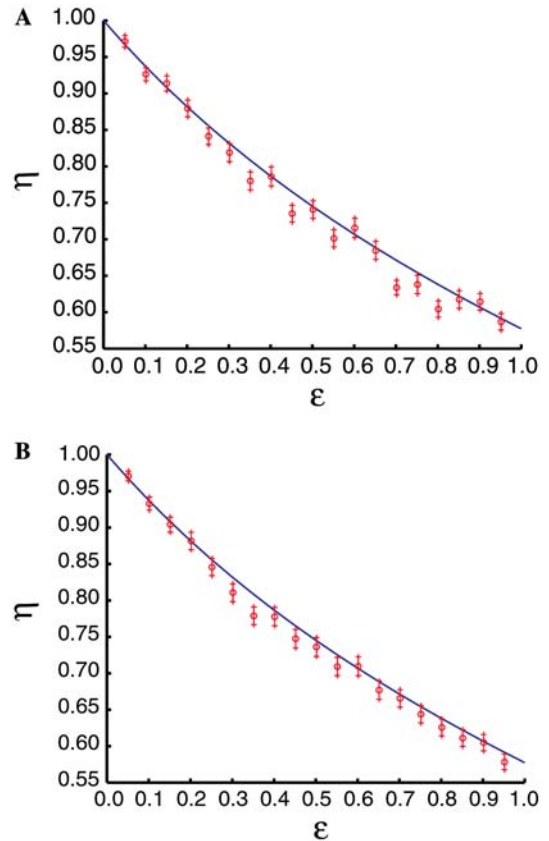
Fig. 3. Computation of the bin-averaged η as a function of $\varepsilon = \delta/\Delta$ with $\Delta + \delta$ held constant for the case of permeable cubic domains. The result in (A) is for the case where the cube domain has a half side of 1 μm, the result in (B) is for the case where the cube has a half side of 1 mm. The $\langle\eta\rangle$ values (red circles) were computed as for Fig. 2, as described in the Methods section. The ideal curve for η at $\chi = 1$, $\eta = \sqrt{(\Delta - \delta/3)/(\Delta + \delta)}$, is given for reference (solid blue line).

t_{exp} (green continuous line). The results in Fig. 5A also indicate that, already for $a = 10$ μm, the blue stars are already stabilizing, and that they are stabilizing very close to the green line and very far from the red line. This is further indication by the simulations that even in the restricted case, the diffusion time assigned to the experiment should be t_{exp} and not t_r.

4.4. Simulated q-space imaging experiment

For a equal to 5, 10, and 15 μm, the results of the simulated q-space experiment are that the displacement distribution obtained with our altered q-space method is a better fit to the true displacement distribution than the displacement distribution obtained with standard q-space. This improvement is especially true for high values of δ. The results for $a = 10$ μm appear in Fig. 5B, with the green circles representing the fit quality of our q-space method, and the red "plus" signs, the fit quality of the standard q-space method. The results for $a = 5$ and 15 μm are not shown.
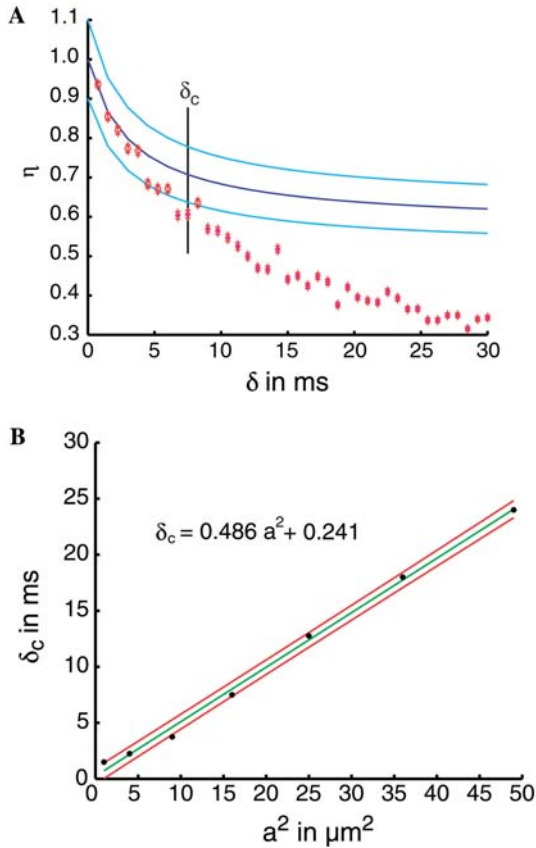
Fig. 4. Computation of the bin-averaged η as a function of δ (in units of ms) with "$\Delta - \delta$" held equal to 5 ms, for the case of a spherical restricted domain. The result in (A) is for the case where the spherical domain has a radius of 4 μm. The $\langle \eta \rangle$ values (red circles) were computed as for Fig. 2, except that we averaged 2000 trajectories (instead of 800), the time for each Markov step was defined so that during t_{exp} there are 2000 Markov steps (instead of being set to 0.1 ms), and the starting point of the trajectory has an equal probability of being anywhere inside a bounding cube of side 8 μm (points outside the spherical domain were not considered). The ideal curve for η at $\chi = 1$, $\eta = \sqrt{(\Delta - \delta/3)/(\Delta + \delta)}$, is given for reference (solid blue line). It can be seen that for a certain δ, the value of $\langle \eta \rangle$ no longer coincides with the ideal curve (blue line). Two cyan bands are then built, one that is equal to 1.1 times the ideal curve and one that is equal to 0.9 times the ideal curve. The time δ_c is equal to the time δ where the $\langle \eta \rangle$ curve has crossed any of the bands twice, and is signaled by a black line with a yellow circle marking the actual simulation result. In (B), we can see the plot of δ_c as a function of the square of the smallest distance to center, a. The black points are the simulation results, the green line is the best linear fit [$\delta_c = 0.486a^2 + 0.241$], and the red lines define a 90% certainty. The slope of the green line is 0.486 and the value at the origin is 0.241.

5. Discussion

Because of limits on $|\mathbf{g}|$ in human MRI [25], the required diffusion sensitivity is typically obtained by increasing δ. Therefore, in human MRI it is common to encounter diffusion-encoding gradients that have a finite duration where the condition $\delta \ll \Delta$ does not apply and sometimes the duration approaches $\delta \approx \Delta$ [11]. In
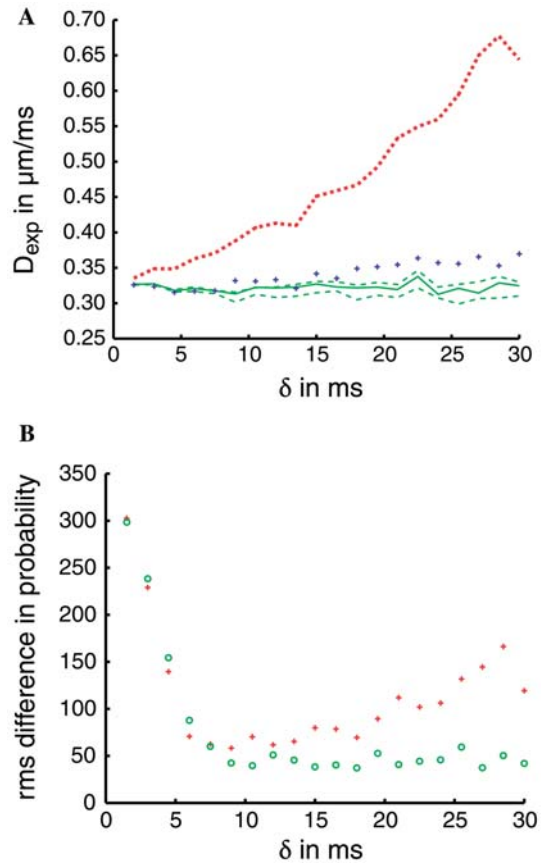
Fig. 5. Computation results for q-space measurements using 32 co-linear different values of q. The simulated diffusion is inside an impermeable sphere of radius $a = 10$ μm. In (A), it is clear that the diffusion coefficient calculated using Eq. (26) (blue "plus" sign) does not approximate the diffusion coefficient calculated using the average square displacement at time t_r (dotted red line), but instead approximates the diffusion coefficient calculated using the average square displacement at time t_{exp} (green continuous line). The dashed green lines are obtained for diffusion times defined by the simulation result expressed in Eq. (27). The results in (B) show the root-mean square error between the true displacement probability (obtained directly from the simulation) and two types of inferred distributions. The red "plus" sign corresponds to the case where the inferred distribution is obtained using a standard 32-points q-space method while considering that the diffusion time is $\Delta - \delta/3$. The green circle corresponds to the case where the inferred probability is obtained by a 32-points q-space Fourier transformation of the MR-signal intensity with $\eta = \sqrt{(\Delta - \delta/3)/(\Delta + \delta)}$.

this work we present a theoretical framework for collecting and analyzing q-space data in the setting of finite-duration diffusion-encoding gradients, while also studying the limitations of the approach in the case of restricted diffusion. By introducing the concept of displacement-specific dephasing, the intrinsic physical displacement probability of a diffusing substance can be linked to the extrinsic effect of the diffusion-encoding gradients on the NMR phase. This provides a solution to the q-space equation that relates the inverse Fourier transform of measured signal attenuations to the

observed probability distribution. The revised q-space equation indicates that $t_{exp} = \Delta + \delta$ must be held constant during the q-space data acquisition, the conventional index **q** should be adjusted by multiplying by the value of the η factor in Eq. (21) prior to Fourier transformation, and the resulting probability is a snapshot of the probability distribution at time $\Delta + \delta$. The latter would be particularly relevant to take into account when interpreting the shape of the measured distribution in terms of sample or tissue microstructure, and when analyzing the dependence of the diffusion coefficient on the diffusion time.

The simulations indicate the validity of Eqs. (21) and (22) that define the cosine dependence of the displacement-specific dephasing $\text{Re}\langle\mathbf{r}|e^{i\phi}\rangle$ for homogeneous and non-homogeneous free Gaussian diffusion, even out to the extremes of $\delta \approx \Delta$. While the fits to simulated data are not perfect, they are within the errors that one would expect given the limitations of simulations due to factors such as width of Z-bins, number of trajectories per bin, etc. It is the existence of this cosine dependence of $\text{Re}\langle\mathbf{r}|e^{i\phi}\rangle$ that enables the inverse Fourier transform to be performed to yield the q-space Eq. (23). Simulations also show validity of the cosine dependence of $\text{Re}\langle\mathbf{r}|e^{i\phi}\rangle$, and thus the capacity to recover the probability with finite-δ q-space imaging, in the case where the sample is composed of macroscopic permeable domains of free Gaussian diffusion (e.g., macroscopic tissue heterogeneity or partial volume effects), as might be expected due to the linear nature of the inverse Fourier transformation. The formalism is valid even in the case where the molecules enter and exit different free-diffusion domains during the experimental diffusion-encoding time.

Simulations also indicate that, in the case of completely impermeable restricted domains, the formalism is valid under some conditions. More specifically, for spheres, the standard MRI settings herein of $\delta \approx 15.75$ ms and $g_z = 18.0$ mT/m would enable q-space probability measurements of restricted cubes as small as $a \approx 4.6\,\mu$m (simulations not shown) and spheres as small as $a \approx 5.7\,\mu$m (based on Figs. 4A and B). A simple doubling of gradient strength would enable δ to be reduced by a factor of 2 for the same q value, which is easily attainable using high-performance clinical gradient hardware. Such an effect would lower the minimum spherical dimension to $a \approx 3$–$3.5\,\mu$m. A general limit of $a > 4\,\mu$m would mean that q-space measurements using these settings could be performed in biological systems that have spherical cells no smaller than a diameter of $\sim 8\,\mu$m. Cells such as neurons have cell bodies larger than this, red blood cells approximate this size, and axonal dimensions are larger than this limit in the longitudinal direction but smaller than this limit in the transverse direction. These are conservative estimates because they assume complete impermeability of the compartment. Most cell membranes have some water

permeability, which may loosen this size requirement. These estimates are only approximate as they are based on the graphs in Fig. 4 where "$\Delta - \delta$" is fixed at 5 ms. Future simulations where δ and "$\Delta - \delta$" are varied simultaneously might better enable the selection of optimal pulse sequence parameters.

Although several papers (e.g., [18,25]) have discussed why finite δ complicates the interpretation of q-space imaging experiments, to our knowledge herein is the first work determining a way to compensate those complications by use of an altered q-space formalism. The capacity to compensate the complications was found to depend on both the size of the restricted domain and the duration of the diffusion-encoding timing parameter.

Changing **q** by changing **g** while keeping δ and Δ fixed (Eq. (25)) allows one to obtain the displacement probability distribution by changing the velocity of spin rotation without altering any other diffusion parameter. This experimental approach was used in [26] and [11]. The results herein indicate that the studies in [11,26] obtain the true displacement probability for the longitudinal axonal direction, but not for the transverse axonal direction. Our formalism also may enable greater experimental flexibility as q-space can be probed in principle by changing δ and Δ, but only if their sum $\Delta + \delta$ is held constant.

Because the data acquired in multi-exponential analyses of diffusion MRI signal intensities is similar to the data used in q-space imaging, this work might also provide some new insights on how to make multi-exponential analysis of DMRI data.

The q-space simulation results obtained that our proposed q-space method works better or just as well as the standard q-space method if $\delta < \delta_c$ (the result for $a = 10\,\mu$m is in Fig. 5B, the result for $a = 15\,\mu$m is not shown). But it was also obtained that, even in the case where $\delta > \delta_c$, our altered q-space method is better at predicting the correct form of the displacement distribution than the standard q-space method (the results for $a = 5\,\mu$m are not shown).

6. Conclusion

A revised formalism for treating q-space data is defined (Eq. (23)) in the case where the condition $\delta << \Delta$ is not met. This formalism is shown to make correct predictions of the displacement distribution for the case of water molecules undergoing a Brownian motion that can be approximated as a Markov process (random walk). The validity of the formalism was confirmed even if the voxel is divided into microscopic regions with different diffusion properties, or if the water molecules are constrained to move in a restricted domain with an impermeable wall (provided the domains are large enough or the diffusion-encoding

timings are short enough). The two types of restricted domains studied were the cube and the sphere, but most of the presented results are for the sphere. The results in Fig. 5B (and other results not shown) are a clear indication that even in the restricted case, our q-space method provides better results than the standard q-space method.

References

[1] E.O. Stejskal, J.E. Tanner, Spin diffusion measurements: spin echoes in the presence of a time dependent field gradient, J. Chem. Phys. 42 (1965) 288–292.

[2] J. Stepisnik, Analysis of NMR self-diffusion measurements by a density matrix calculation, Physica B 104 (1981) 350–364.

[3] L.Z. Wang, A. Caprihan, E. Fukushima, The narrow-pulse criterion for pulsed-gradient spin-echo diffusion measurements, J. Magn. Reson. Series A 117 (1995) 209–219.

[4] W.S. Price, Pulsed-field gradient nuclear magnetic resonance as a tool for studying translational diffusion. 1. Basic theory, Concepts in Magn. Reson. 9 (1997) 299–336.

[5] P.P. Mitra, B.I. Halperin, Effects of finite gradient-pulse widths in pulsed-field-gradient diffusion measurements, J. Magn. Reson. Series A 113 (1995) 94–101.

[6] E.O. Stejskal, Use of spin echoes in a pulsed magnetic-field gradient to study anisotropic, restricted diffusion and flow, J. Chem. Phys. 43 (1965) 3597–3603.

[7] P.T. Callaghan, Pulsed field gradient nuclear magnetic resonance as a probe of liquid state molecular organization, Aus. J. Phys. 37 (1984) 359–387.

[8] D.G. Cory, A.N. Garroway, Measurement of translational displacement probabilities by NMR: an indicator of compartmentation, Magn. Reson. Med. 14 (1990) 435–444.

[9] P.T. Callaghan, D. MacGowan, K.J. Packer, F.O. Zelaya, High-resolution q-space imaging in porous structures, J. Magn. Reson. 90 (1990) 177–182.

[10] P.T. Callaghan, A. Coy, D. MacGowan, K.J. Packer, F.O. Zelaya, Diffraction-like effects in NMR diffusion studies of fluids in porous solids, Nature 351 (1991) 467–469.

[11] Y. Assaf, D. Ben-Bashat, J. Chapman, S. Peled, I.E. Biton, M. Kafri, Y. Segev, T. Hendler, A.D. Korczyn, M. Graif, Y. Cohen, High b-value q-space analyzed diffusion-weighted MRI: application to multiple sclerosis, Magn. Reson. Med. 47 (2002) 115–126.

[12] M.H. Blees, The effect of finite duration of gradient pulses on the pulsed-field-gradient NMR method for studying restricted diffusion, J. Magn. Reson. Series A 109 (1994) 203–209.

[13] P.T. Callaghan, S.L. Codd, J.D. Seymour, Spatial coherence phenomena arising from translational spin motion in gradient spin echo experiments, Concepts Magn. Reson. 11 (1999) 181–202.

[14] N.F. Lori, Diffusion Tensor Tracking of Neuronal Fiber Pathways in the Living Human Brain. Physics, Washington University, St. Louis, 2001.

[15] P.T. Callaghan, NMR imaging, NMR diffraction and applications of pulsed gradient spin echoes in porous media, Magn. Reson. Imag. 14 (1996) 701–709.

[16] P.T. Callaghan, A simple matrix formalism for spin echo analysis of restricted diffusion under generalized gradient waveforms, J. Magn. Reson. 129 (1997) 74–84.

[17] A. Caprihan, L.Z. Wang, E. Fukushima, A multiple-narrow-pulse approximation for restricted diffusion in a time-varying field gradient, J. Magn. Reson. Series A 118 (1996) 94–102.

[18] J. Stepisnik, Validity limits of Gaussian approximation in cumulant expansion for diffusion attenuation of spin echo, Phys. B 270 (1999) 110–117.

[19] N.F. Lori, T.E. Conturo, Diffusion time assignment and q-space formalism for finite-duration diffusion-encoding gradients: Simulation of 3D random walks, Diffusion MRI: Biophysical issues, Saint-Malo, France, 10–12 March 2002, pp. 9–12.

[20] P.T. Callaghan, J. Stepisnik, Generalized analysis of motion using magnetic field gradients, in: Advances in Magnetic and Optical Resonance, Academic Press, San Diego, 1996, pp. 325–388.

[21] T.Q. Li, M. Haggkvist, L. Odberg, Porous structure of cellulose fibers studied by Q-space NMR imaging, Langmuir 13 (1997) 3570–3574.

[22] D.A. McQuarrie, Statistical Mechanics, University Science Books, Sausalito, CA, 2000.

[23] E.W. Weisstein, CRC Concise Encyclopedia of Mathematics, CRC Press LLC, Boca Raton, FL, 1998.

[24] J.S. Shimony, R.C. McKinstry, E. Akbudak, J.A. Aronovitz, A.Z. Snyder, N.F. Lori, T.S. Cull, T.E. Conturo, Quantitative diffusion-tensor anisotropy brain MR imaging: normative human data and anatomic analysis, Radiology 212 (1999) 770–784.

[25] P.J. Basser, Relationships between diffusion tensor and q-space MRI, Magn. Reson. Med. 47 (2002) 392–397.

[26] D.S. Tuch, Diffusion MRI of Complex Tissue Structure. Radiological Sciences, Massachusetts Institute of Technology, Cambridge, MA, 2002.